



# Orientation of Nd and Mn magnetic moments in a CMR $\text{Nd}_{0.72}\text{Ba}_{0.28}\text{MnO}_3$ by X-ray magnetic circular dichroism

O. Toulemonde<sup>a</sup>, F. Studer<sup>a,\*</sup>, A. Llobet<sup>b</sup>, L. Ranno<sup>b</sup>, A. Maignan<sup>a</sup>, E. Pollert<sup>c</sup>,  
M. Nevriva<sup>c</sup>, E. Pellegrin<sup>d</sup>, N.B. Brooks<sup>e</sup>, J. Goedkoop<sup>e</sup>

<sup>a</sup>CRISMAT, ISMRA, Boulevard Maréchal Juin, 14050 Caen Cedex, France

<sup>b</sup>Laboratoire de Magnétisme Louis Néel, CNRS-BP 166, F-38042 Grenoble Cedex 09, France

<sup>c</sup>Laboratory of Oxidic Materials, Institute of Physics, 162 53 Prague 6, Czech Republic

<sup>d</sup>Forschungszentrum Karlsruhe, ANKA P.O. Box 3640, D-76021 Karlsruhe, Germany

<sup>e</sup>ESRF, BP 220, 38043 Grenoble Cedex, France

Received 23 January 1998; received in revised form 30 April 1998

## Abstract

X-ray absorption and X-ray magnetic circular dichroism at Mn  $L_{2,3}$ - and Nd  $M_{4,5}$ -edges of a twinned  $\text{Nd}_{0.72}\text{Ba}_{0.28}\text{MnO}_3$  single crystal have been performed versus temperature (between 10 and 300 K) and applied magnetic field (between 0 and 6.5 T). The results show that neodymium cations order below 70 K with the magnetic moments antiparallel to the manganese subnetwork in weak applied magnetic field (<1.5 T). For higher magnetic field, the neodymium moments turn parallel to the manganese ones showing that the antiferromagnetic exchange coupling between both subnetworks is weak. The presence of a metal–insulator transition below 70 K in the studied single crystal correlated to the magnetic ordering of neodymium cations can be understood on the basis of the cation mismatch introduced by barium substitution. © 1998 Elsevier Science B.V. All rights reserved.

PACS: 78.70.Dm; 75.70.Pa

Keywords: X-ray absorption and absorption edges; Giant magnetoresistances

## 1. Introduction

Since the discovery of their colossal magneto-resistance properties (CMR), manganese perovskites  $(\text{Ln}_{1-x}\text{A}_x)\text{MnO}_3$  (Ln being a trivalent lanthanide

and A a divalent cation) have been extensively studied [1–9]. For  $x$  less than 0.5, the  $(\text{Ln}_{1-x}\text{A}_x)\text{MnO}_3$  manganites exhibit generally a simple paramagnetic to ferromagnetic transition although, for a composition like  $\text{Pr}_{0.7}(\text{Ca}_{0.3-x}\text{Sr}_x)\text{MnO}_3$  and for  $x$  less than 0.05, the insulating behavior is kept down to 5 K and the PM–FM transition is induced only by applying a magnetic field [10–13].

\* Corresponding author. Tel.: + 31-45-26-70; fax: + 31-95-16-00; e-mail: studer@crindy.ismra.fr.

The first parameter, which has been considered to explain the dependence of the electron transport and magnetic properties on the nature of the substituted cation (Ca, Sr, Ba), is the average size of the A site cation of the perovskite  $\langle r_A \rangle$  [13–16]. It has been shown that  $T_c$ , which characterizes the PM–FM transition, increases regularly with  $\langle r_A \rangle$  in the range 1.221–1.263 Å. In a recent study of the  $\text{Ln}_{0.7}\text{A}_{0.3}\text{MnO}_3$  compounds, Rodriguez–Martinez et al. [17] revealed that a second factor, the mismatch effect, influences significantly  $T_c$ . This effect is represented by the variance of the A cations radii distribution,  $\sigma^2$ , which quantifies the random disorder of  $\text{Ln}^{3+}$  and  $\text{A}^{2+}$  cations distributed over the A site of the perovskite.

On the other hand, the existence of a magnetic moment on neodymium below 35 K, parallel to the magnetic moments of the manganese subnetwork, has been shown in the  $\text{Nd}_{0.7}\text{A}_{0.3}\text{MnO}_3$  (A = Ca, Sr) compounds by Millange et al. [18,19] using neutron diffraction. These observations allowed one to think about the influence of the neodymium moments on the magnetic ordering and hence on the electronic transport properties of these manganites. The synthesis of single crystals with composition  $\text{Nd}_{0.72}\text{Ba}_{0.28}\text{MnO}_3$  allowed to investigate simultaneously the relative magnetic ordering of both neodymium and manganese subnetworks correlated to the electron transport properties in a barium compound for which the mismatch effect must be very large.

Here, we present an investigation of the magnetic ordering on neodymium and manganese subnetworks of  $\text{Nd}_{0.72}\text{Ba}_{0.28}\text{MnO}_3$  single crystals by X-ray absorption (XAS) and magnetic X-ray circular dichroism (MXCD) at Mn  $L_{2,3}$ - and Nd  $M_{4,5}$ -edges as a function of temperature and applied magnetic field.

## 2. Experimental

Single crystals with composition  $\text{Nd}_{0.72}\text{Ba}_{0.28}\text{MnO}_3$  were prepared by a flux growth method from the melt containing (0.41 BaO–0.18 BaF<sub>2</sub>–0.41 B<sub>2</sub>O<sub>3</sub>)–NdMnO<sub>3</sub> [20]. Dark orthorhombic shaped crystals were grown in the

temperature range 1160–900°C using a cooling rate of 0.5–1 K/h.

Electron probe micro-analysis of the crystal was performed with a Phillips FEG-XL30 scanning electron microscope equipped with EDS-LINK analysis system to confirm the cation composition at 10%.

The nuclear and magnetic structure of a ceramic sample exhibiting a close composition  $\text{Nd}_{0.7}\text{Ba}_{0.3}\text{MnO}_3$  has been realized by powder neutron diffraction between 1.5 and 300 K at ILL (Grenoble) [21].

Magnetization measurements were made with a superconducting quantum interference device SQUID (MPMS, Quantum Design) and with a PAR vibrating sample magnetometer.

Magnetoresistance measurements were made with conventional four probe DC with a physical property measuring system (PPMS, Quantum Design). Electrical contacts were made by ultrasonic soldering of indium on the surface of the crystal. Note that all magnetic and magnetoresistance measurements were carried out during a zero-field cooled warming (ZFCW) process.

X-ray absorption spectra at Mn  $L_{2,3}$ - and Nd  $M_{4,5}$ -edges were recorded using circular polarized light at the Dragon beamline (ID12b) of the ESRF (Grenoble, France) and at beamline SU23 at Lure (Orsay, France) both in the total electron yield mode. At LURE, Nd  $M_{4,5}$ -edges were recorded using the second-order light. All the spectra were recorded after a zero-field cooled process and the sample was scraped in situ before the measurements. The base pressure in the spectrometer chamber was  $2.3 \times 10^{-9}$  mbar at the ESRF and  $1.6 \times 10^{-9}$  mbar at LURE when the sample was cleaved or scraped.

At LURE and ESRF, the same single crystal was used. At ESRF it was cleaved in situ but the rough and step-like look of the sample surface prevented any specific crystallographic orientation to be considered. At LURE it was scraped in situ. Then energy scans were realized for each direction of the applied magnetic field (parallel and antiparallel to the direction of the wave vector of incoming photons) for a fixed helicity of the light (right polarization).

For the calibration between LURE and ESRF experiments, two spectra were recorded at Mn

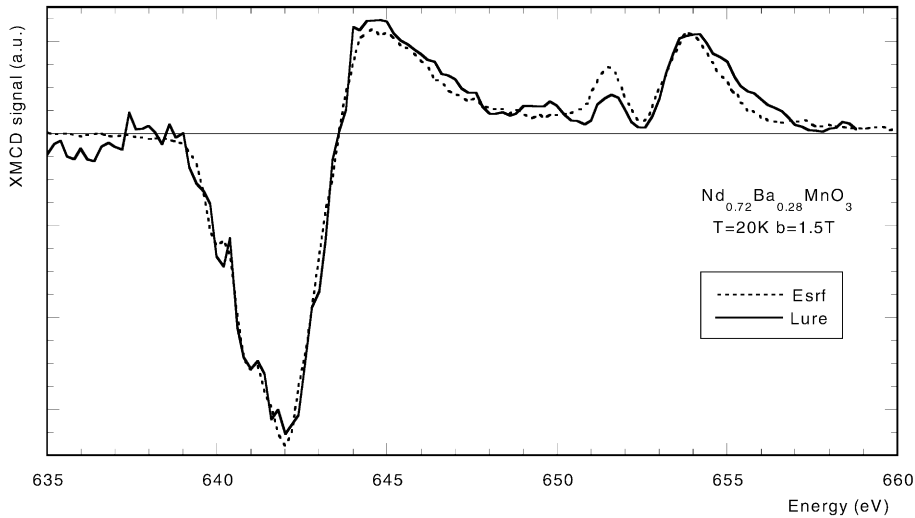


Fig. 1. Normalization of dichroism spectra recorded at Mn  $L_3$ -edge at LURE and at ESRF in the same experimental conditions.

$L_{2,3}$ -edge at  $T = 20$  K and for an applied magnetic field equal to  $\pm 1.5$  T (Fig. 1). To account for various polarization rates (ESRF  $\approx 85\%$ ; LURE  $\approx 65\%$ ) and absorption yield between both experiments, X-ray absorption spectra and XMCD signal recorded at LURE were, respectively, multiplied by factors of 8 and 18 in order to be compared with those recorded at the ESRF. The difference in XAS and XMCD yields between ESRF and LURE experiments may be due to the deteriorated surface state of the scraped sample compared to the cleaved one.

### 3. X-ray magnetic circular dichroism

Magnetic circular X-ray dichroism has proven to be a valuable probe of the local magnetic properties of ferromagnetic or ferrimagnetic materials [22–25]. The XMCD signal is defined as the absorption difference  $I_{\text{XMCD}} = \mu^+ - \mu^-$  where  $\mu^+$  and  $\mu^-$  are the absorption cross-sections of the sample when the magnetic field is applied parallel and antiparallel, respectively, to the propagation direction of the X-rays with fixed circular polarization.

XMCD benefits from the double selectivity of the X-ray absorption spectroscopy: it is sensitive to the chemical species of the absorbing atom and to

the symmetry of the unoccupied electronic state probed by the photoelectron taking into account the electric dipole selection rules.

The XMCD signal is directly proportional to the value of the magnetic moment carried by the orbital shell of the element probed by the dipolar electric transitions at the edge chosen.

The so-called ‘sum rules’ introduced by Thole and Cara [26,47] allows to distinguish between the projections of the orbital magnetic moment  $\langle L_z \rangle$  and the spin magnetic moment  $\langle S_z \rangle$  contributing to the total magnetic moment vector  $\langle M_z \rangle$  for each probed element and edge. In our study of the transition  $2p^{1/2} \rightarrow 3d$  and  $2p^{3/2} \rightarrow 3d$  on manganese atoms, the orbital magnetic moment (in  $\mu_B/\text{atom}$ ) is given by the first sum rule:

$$m_{\text{orbital}} = - \frac{4 \int_{L_3+L_2} (\mu_+ - \mu_-) d\omega}{3 \int_{L_3+L_2} (\mu_+ + \mu_-) d\omega} (10 - n_{3d})$$

and the spin magnetic moment in units of  $\mu_B/\text{atom}$  is given by the second sum rule:

$$m_{\text{spin}} = - \frac{6 \int_{L_3} (\mu_+ - \mu_-) d\omega - 4 \int_{L_3+L_2} (\mu_+ - \mu_-) d\omega}{\int_{L_3+L_2} (\mu_+ + \mu_-) d\omega} \times (10 - n_{3d}) \left( 1 + \frac{7 \langle T_z \rangle}{2 \langle S_z \rangle} \right)^{-1},$$

where  $n_{3d}$  is the 3d electron occupation number of manganese and  $L_3$  and  $L_2$  denote the integration range,  $\langle T_z \rangle$  is the expected value of the magnetic dipole operator and  $\langle S_z \rangle = 1/2m_{\text{spin}}$  in Hartree atomic units. Ratio  $\langle T_z \rangle / \langle S_z \rangle$  was shown to be negligible in the case of transition metal atoms at room temperature [27]. But analytical calculations of  $\langle T_z \rangle$  for  $\text{Cu}^{2+}$  in the octahedral field also showed that its value can be larger than  $S_z$  at low temperature [28,48].

Therefore, one should be able to deduce from the XMCD signal qualitative information on the relative orientation of magnetic moments carried by various elements within the sample and also quantitative information on the magnetic moments  $\langle M_z \rangle = (\langle L_z \rangle + 2\langle S_z \rangle)\mu_B$  using the sum rules provided that a calculation of  $T_z$  is performed. Thus, the second sum rule allows an estimation of the manganese spin contribution  $\langle S_z \rangle$  provided that the  $L_3$ - and  $L_2$ -edges are well separated. But, in the case of manganese oxides, the spin-orbit splitting of the core hole is not large enough to prevent a mixing of the  $J$  contributions to the  $L_3$ - and  $L_2$ -edges such that error in the determination of  $\langle S_z \rangle$  as large as 200% has been shown by the multiplet calculations [29].

## 4. Results and discussion

### 4.1. Transport measurement

Fig. 2 shows the temperature dependence of the resistance at various magnetic field. At  $T_{\text{max}} = 140$  K, the zero-field curve exhibits a first transition from a semi-conducting state ( $dR/dT < 0$ ) to a metallic state ( $dR/dT > 0$ ) and a second from a metallic to a semi-conductor state below 55 K.

The magnetoresistance ratio (Fig. 3) increases with the applied magnetic field: the higher the magnetic field, the larger is the ratio  $R(H=0)/R(H)$ . Whatever the magnetic field, the magnetoresistance peak takes place at  $T = 140$  K which corresponds to the  $T_{\text{max}}$  transition temperature from a semi-conducting to a metallic state without field.

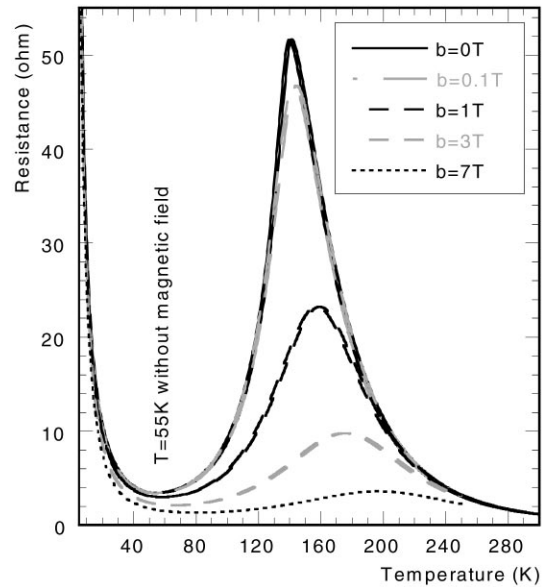


Fig. 2. Thermal variation of the resistance of the sample  $\text{Nd}_{0.72}\text{Ba}_{0.28}\text{MnO}_3$  at different magnetic fields.

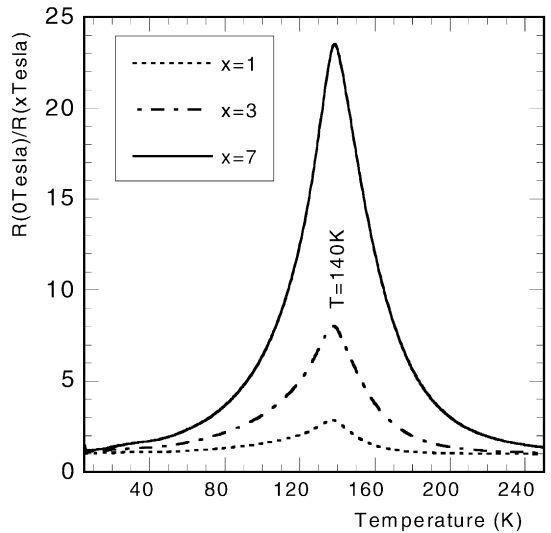


Fig. 3. Thermal variation of the magnetoresistance ratio of the sample  $\text{Nd}_{0.72}\text{Ba}_{0.28}\text{MnO}_3$  at different magnetic fields.

### 4.2. Magnetization measurement

Fig. 4 shows the temperature dependence of the magnetization for various magnetic fields. The

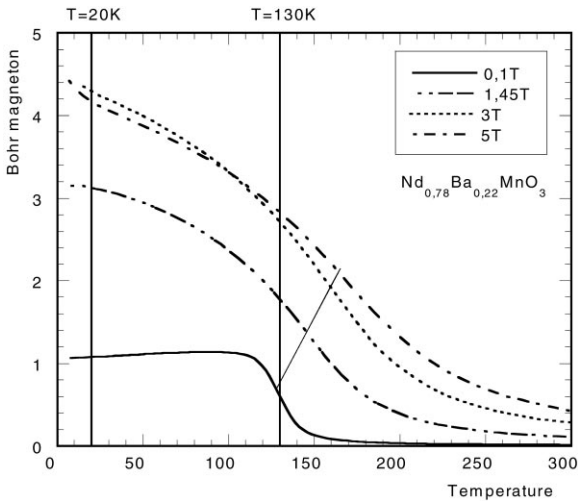


Fig. 4. Thermal variation of the magnetization of the sample  $\text{Nd}_{0.72}\text{Ba}_{0.28}\text{MnO}_3$  at different magnetic fields. Lines are drawn at temperature at which XMCD spectra were recorded and between inflection points taken as  $T_c$ 's.

Table 1

Magnetic field (T)	Curie temperature (K)	Maximum resistivity temperature (K)
0, 1	128	143
1, 45	144	160
3	160	177
5	165	197

parallelepiped shape allowed us not to take into account the demagnetizing field effect. The magnetic transition Curie temperatures  $T_c$ , from the paramagnetic to the ferromagnetic state increase, with the applied magnetic field and are in reasonable agreement with the corresponding  $T_{\text{max}}$  (Table 1). The transition width also increases strongly with the applied magnetic field as usually observed in the CMR rare earth manganites and is likely due to the distribution of magnetic moments induced by a variable energy spread of magnetic polarons [30].

The projection on the quantification axis of the molar saturation magnetization of  $\text{Nd}_{0.72}\text{Ba}_{0.28}\text{MnO}_3$  at low temperatures estimated for  $\text{Nd}^{3+}$  is  $0.4 \mu_B$  as shown from neutron diffraction [21] while, for high spin  $\text{Mn}^{3+}$  with orbital

contribution quenched, the moment can be calculated as  $\mu_{\text{Mn}} = 2\mu_B[0.72*2 \text{ (for Mn}^{3+}) + 0.28*3/2 \text{ (for Mn}^{4+})] = 3.72 \mu_B$  – the amount of  $\text{Mn}^{4+}$  species (0.28) being fixed by the barium substitution rates. Thus, a simple model of  $\text{Nd}^{3+}$  and  $\text{Mn}^{3+}$  ferromagnetic sublattices will predict a zero temperature magnetization of  $3.43 \mu_B$  if the two sublattices are antiparallel and  $4.01 \mu_B$  if the two sublattices are parallel. The magnetization curve at 5 T and  $T = 20$  K shows a zero temperature magnetization which is in better agreement with a scenario including two ferromagnetically aligned sublattices.

#### 4.3. X-ray absorption spectroscopy

X-ray absorption spectra at the Mn  $L_{2,3}$ -edges were recorded between 635 and 680 eV with circular polarized light. After removal of the linear background estimated between 635 and 637 eV, spectra are normalized to unity at the top of manganese  $L_3$ -edge.

Fig. 5 shows X-ray absorption spectra at the Mn  $L_3$ -edge at various temperatures. As already

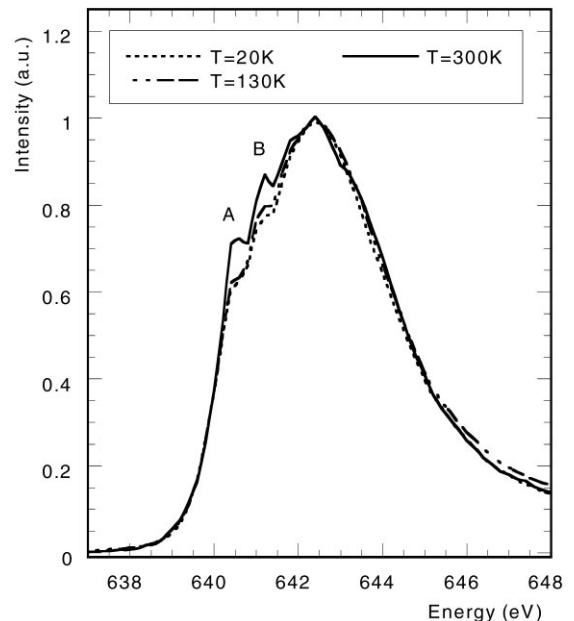


Fig. 5. Mn  $L_3$ -edges of  $\text{Nd}_{0.72}\text{Ba}_{0.28}\text{MnO}_3$  in zero magnetic field for the three studied temperatures showing the change in intensity of shoulder A and B below  $T_c$  ( $T_c = 140$  K).

observed in  $\text{Pr}_{0.7}\text{Sr}_{0.3}\text{MnO}_3$  compound [31], shoulders A and B decrease in intensity at the transition from the paramagnetic–semiconducting state to the ferromagnetic–metallic state. Shoulder A corresponds to a  $\text{Mn}^{3+}$  ( $3d^4$ ) high spin cation and shoulder B to  $\text{Mn}^{4+}$  ( $3d^3$ ) as shown in Fig. 6. Manganese  $3d^4$  low spin and manganese  $3d^4$  high spin were calculated by de Groot using a charge transfer multiplet model [32] based on the crystallographic data of  $\text{LiMnO}_2$ . The absence of the so-called A peak at 641 eV in the calculated spectrum of  $\text{Mn}^{3+}$  ( $3d^4$ ) low spin allows one to think that the introduction of some amount of low-spin contribution could decrease the A shoulder intensity. Conversely, the existence of a pre-peak at 640 eV, also characteristic of the low spin contribution, does not appear clearly in the sum of the three

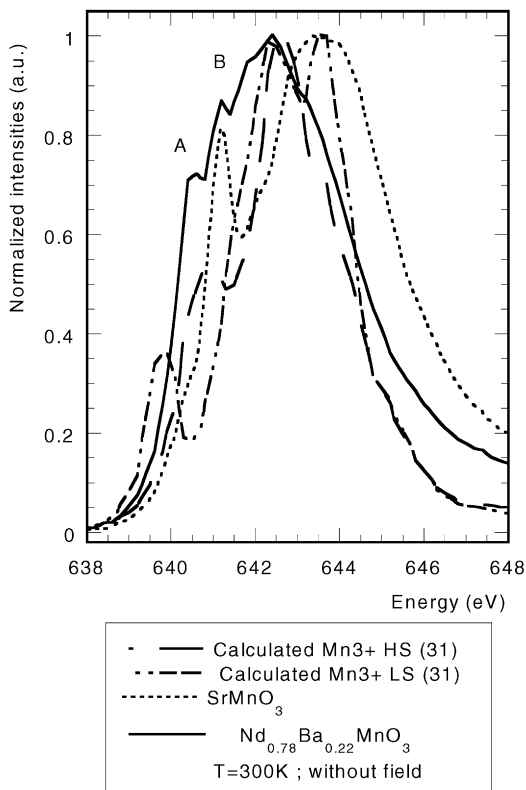


Fig. 6. Observed Mn  $L_3$ -edges for  $\text{SrMnO}_3$  and  $\text{Nd}_{0.72}\text{Ba}_{0.28}\text{MnO}_3$  at room temperature and TT-multiplet simulation of octahedral  $\text{Mn}^{3+}$  high and low spin from De Groot [32].

contributions for a small amount of low spin configuration ( $<25\%$ ) [31].

However, a decrease of shoulders A and B is observed at low temperature 20 and 130 K with respect to room temperature. This could be explained by the introduction of some amount of low spin contribution which could in turn be explained by a crystal field change at  $T_{\text{max}}$  related to a decrease of the Jahn–Teller distortion. Variations of the Jahn–Teller distortion have been observed by powder neutron diffraction in some manganites but remain often weak [33–37]. Specially, in the case of the neighbor  $\text{Nd}_{0.7}\text{Ba}_{0.3}\text{MnO}_3$  [21] compound, powder neutron diffraction has shown little change in the Mn–O distances between 250 and 1.5 K. However, the large changes observed at Mn  $L_3$ -edge may be attributed to a strong dynamical Jahn–Teller effect as proposed by Millis et al. [38,49].

#### 4.4. X-ray magnetic circular dichroism

To extract the XMCD signal from X-ray absorption spectra recorded with right-hand polarized light, one must be sure that both spectra, recorded with the magnetic field parallel and antiparallel to the direction of the wave vector of the incoming photons, can be superposed at low (635 eV) and high energy (680 eV). To obtain this superposition, one of the spectra can be multiplied by a constant which originates from the natural decrease of the beam light intensity between spectra with reversed magnetic field directions.

To proceed with the calculation of the sum rules, the total signal  $\mu_{\text{tot}}$  was obtained by adding up the XAS spectra recorded with the magnetic field parallel and antiparallel to the direction of the X-ray beamline. Then, after removal of the linear background estimated between 635 and 637 eV, a two-step-like function for edge removal was subtracted before the integration. We have set the first step of the function to 0.667 and the second one to unity at 667 eV. This point was shown previously by Pellegrin [39] to be equal to one after normalization, the normalization being determined at higher energy ( $>720$  eV).

Fig. 7 shows the Mn  $L_{2,3}$ -edges of a  $\text{Nd}_{0.72}\text{Ba}_{0.28}\text{MnO}_3$  single crystal recorded at 6.5 T

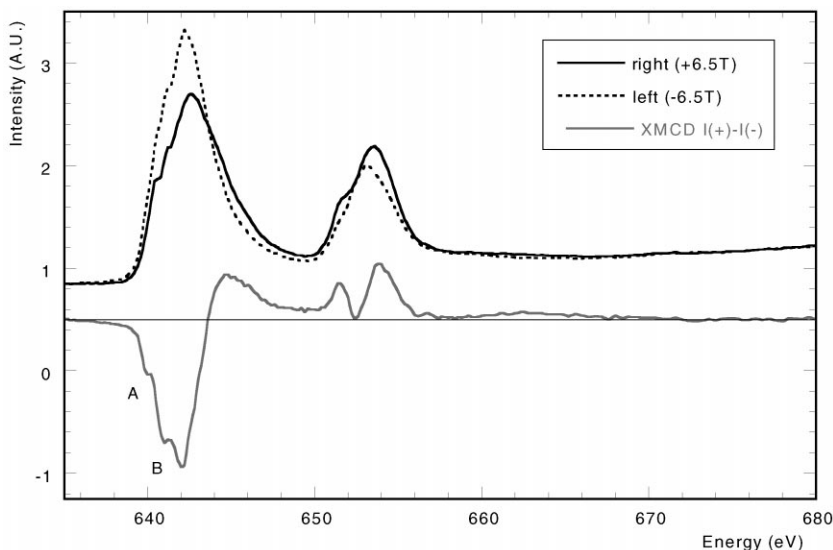


Fig. 7. XMCD signal of  $\text{Nd}_{0.72}\text{Ba}_{0.28}\text{MnO}_3$  at Mn  $L_3$ -edge at  $T = 20$  K.

and  $T = 20$  K and the corresponding dichroic signal obtained at ESRF. A similar treatment was used throughout this work for Mn  $L_{2,3}$ - and Nd  $M_{4,5}$ -edges.

The strong negative peak at about 642 eV already observed by Pellegrin [39] exhibits two shoulders A and B. These shoulders correspond to the ones observed on the XAS spectra (Fig. 6). In agreement with the above assignment shoulder B is due to  $\text{Mn}^{4+}$  ( $3d^3$ ) and the shoulder A seems to be linked to the presence of an  $\text{Mn}^{3+}$  ( $3d^4$ ) high spin state.

The first qualitative but important information that can be drawn from XMCD signals is the relative orientation of both Nd and Mn magnetic subnetworks. Note that the direction of the magnetic moment carried by the manganese cations follows the magnetic field (Fig. 8). Then, whatever the temperature and the magnitude of the applied magnetic field are, magnetic moment carried by the manganese cations stay parallel to the direction of propagation vector of the soft X-rays and on the same way. At Nd  $M_{4,5}$ -edge Goedkoop et al. [40] reported calculated XMCD signals for right hands circular polarization similar to our spectra recorded at 6.5 T and 1.5 T (Fig. 9a). It is worth noting here that due to the small magnetic moment

of the Nd cation, the  $M_5$ -edge dichroic signal disappears in the noise and that only the more intense  $M_4$ -edge dichroic signal can still be observed in low magnetic fields, below 1.5 T. Since the XMCD signals were calculated for a magnetic moment carried by the neodymium cation parallel to the direction of the applied magnetic field, one can conclude a parallel ordering of manganese and neodymium magnetic moments for applied magnetic fields at least equal to or higher than 1.5 T at  $T = 20$  K.

On the other hand at  $T = 20$  K an antiparallel ordering of manganese and neodymium magnetic moments can be concluded from the fact that the XMCD signal at the Nd  $M_4$ -edge at 0.1 T is reversed compared to the one at the Nd  $M_4$ -edge at 6.5 T (Fig. 9b). An antiparallel ordering between the manganese and the rare earth sublattices has already been seen in  $\text{Gd}_{0.67}\text{Ca}_{0.33}\text{MnO}_3$  [41] and  $\text{Nd}_{0.7}\text{Ba}_{0.3}\text{MnO}_3$  [21] compounds by powder neutron diffraction without field. In the latter paper, the projection on the quantification axis of the magnetic moment of the Nd cation has been estimated to be  $0.4 \mu_B$ . This antiparallel ordering has been observed for the first time either by neutron diffraction and XMCD in neodymium barium manganite for substitution amount between 0.25 and 0.3. For the same composition, in the cases of

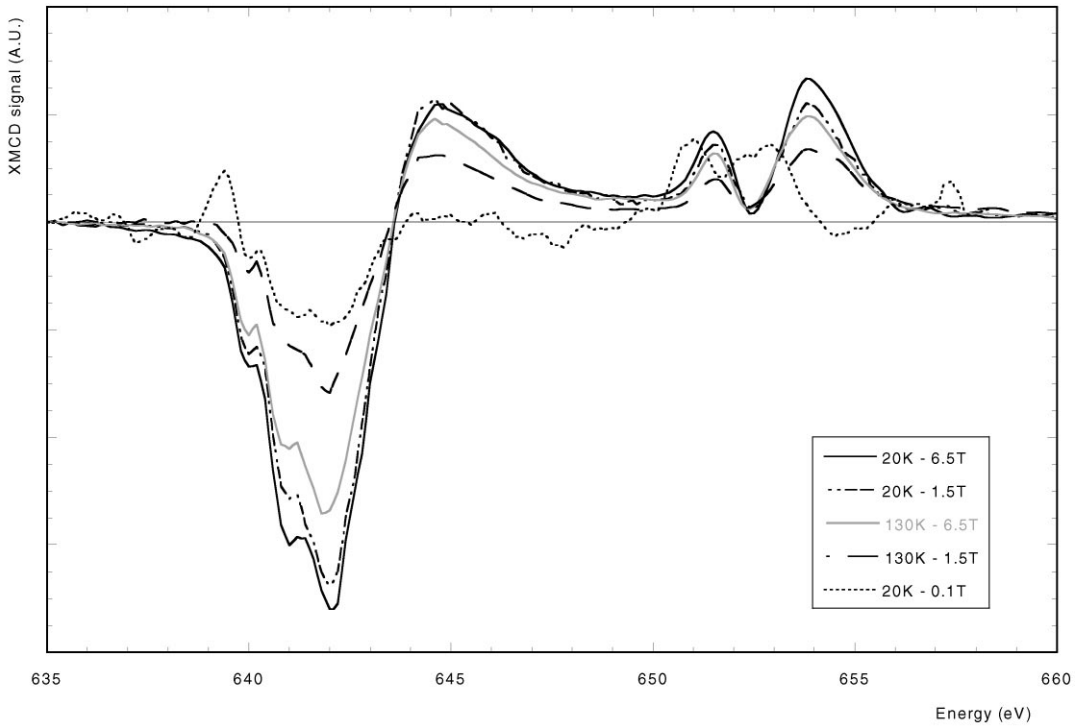


Fig. 8. XMCD signals versus temperature and applied magnetic field.

Ca and Sr substitution, a parallel ordering of neodymium and manganese subnetworks has always been observed by neutron diffraction experiments [18,19].

In high field (6.5 T), the XMCD signal at Nd  $M_{4,5}$ -edge is shown for different temperatures in Fig. 10. A dichroic signal and thus a magnetic moment can still be seen on the neodymium cation at  $T = 40$  K and  $H = 6.5$  T. Fig. 11 shows the decrease of the XMCD signal at 1000.6 eV and its extrapolation to higher temperatures. This extrapolation shows that the XMCD signal at Nd  $M_{4,5}$ -edge disappears above 75 K assuming a linear variation of the Nd sublattice magnetization. Moreover, a parallel ordering between both manganese and neodymium sublattices in high magnetic field is in agreement with the value of the magnetization ( $4.12 \mu_B$ ) recorded at 5 T (Fig. 4).

On the resistance curve (Fig. 2), a second transition from metallic to a semi-conducting state takes place below 55 K without field and below

80 K at 7 T. Such metallic to semi-conducting behavior is already observed at low temperature upon cooling on  $\text{La}_{1-x}\text{Sr}_x\text{MnO}_3$  ( $0.14 < x < 0.16$ ) without applied magnetic field [42] but it is visible neither on the resistance curves of the powder  $\text{Nd}_{0.7}\text{Ba}_{0.3}\text{MnO}_3$  [43] sample nor for calcium and strontium substitution of the neodymium manganite [44]. A few hypotheses can be proposed to account for this particular behavior in the single crystal which is twinned as usual in these distorted perovskite structures.

The first one is based on the existence at the twin boundaries of a second phase slightly different in stoichiometry and exhibits a metallic to semi-conducting transition at low temperature. But, it is likely that such a second phase should occur also at the grain boundaries in the case of the powder samples which do not show any transition at low temperature.

The second one is based on the existence of charge ordering on the manganese lattice as it is

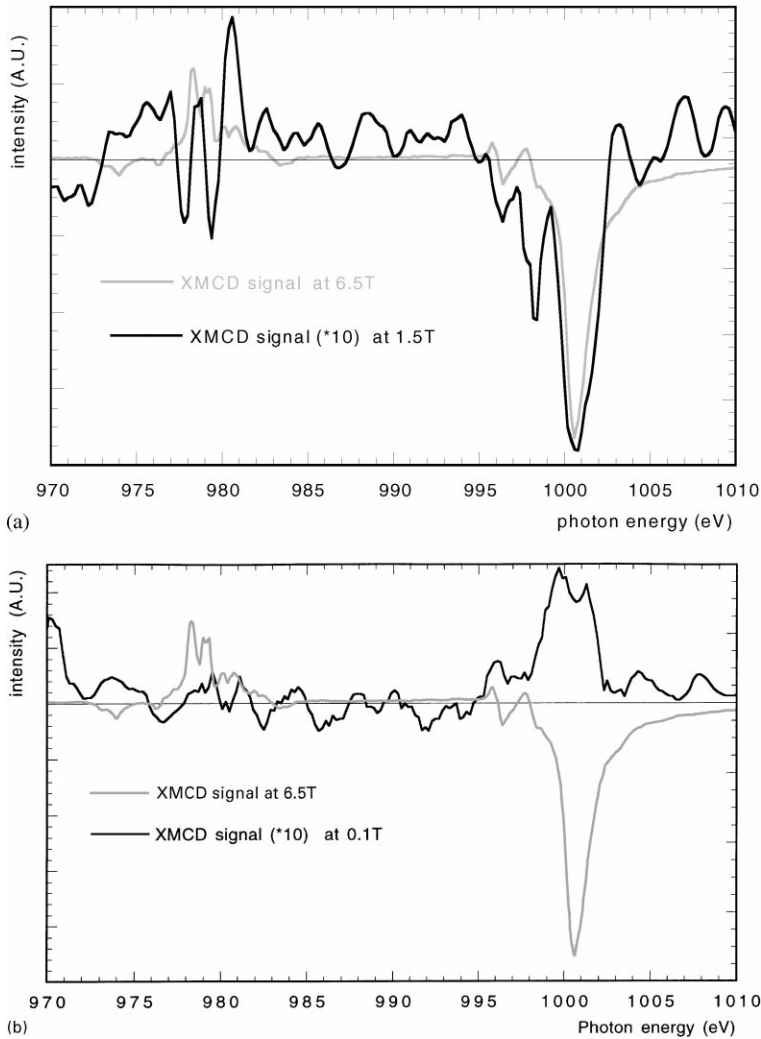


Fig. 9. (a) XMCD signals of  $\text{Nd}_{0.72}\text{Ba}_{0.28}\text{MnO}_3$  at Nd  $M_{4/5}$ -edge at  $T = 20$  K for  $b = 6.5$  and  $1.5$  T. (b) XMCD signals of  $\text{Nd}_{0.72}\text{Ba}_{0.28}\text{MnO}_3$  at Nd  $M_{4/5}$ -edge at  $T = 20$  K for  $b = 6.5$  and  $0.1$  T.

observed for  $\text{Nd}_{0.7}\text{Ca}_{0.3}\text{MnO}_3$  compound [19]. This charge ordering phenomenon might be linked with a magnetic ordering on the neodymium sublattice. Our experiments tend to show that the magnetic moments on neodymium and the transition from metallic to semi-conductor state, below 60 K without field and below 80 K at 7 T, are correlated. But, considering the cation size mismatch effect on the A site [17,45], the mismatch at the A site, introduced by replacing  $\text{Nd}^{3+}$  ion ( $r = 1.27 \text{ \AA}$ ) [46] by  $\text{Ba}^{2+}$  ion ( $r = 1.61 \text{ \AA}$ ) is larger

than the one induced by replacing  $\text{Nd}^{3+}$  ion by  $\text{Ca}^{2+}$  ( $r = 1.34 \text{ \AA}$ ) ion. A charge ordering phenomenon is thus more likely on  $\text{Nd}_{0.7}\text{Ca}_{0.3}\text{MnO}_3$  compound than on  $\text{Nd}_{0.72}\text{Ba}_{0.28}\text{MnO}_3$ . One can also consider that the transition from metallic to semi-conductor state is linked to this cation size mismatch effect.

The third one is based on the existence of a phase transition in the  $\text{Nd}_{0.72}\text{Ba}_{0.28}\text{MnO}_3$  twinned single crystal itself which would lead the magnetic ordering on the neodymium sublattice and the metallic

to semi-conducting behavior. The question raised here is whether or not this phase transition could be observed by neutron diffraction of the  $\text{Nd}_{0.72}\text{Ba}_{0.28}\text{MnO}_3$  twinned single crystal.

At Mn  $L_{2,3}$ -edge, whatever the magnetic field, no XMCD signal at 300 K could be observed in agreement with the paramagnetic state. The XMCD signal starts to be observed at 130 K, temperature close to  $T_c$  as observed on magnetization curves. Then the XMCD signal (Fig. 9) increases with decreasing temperatures and increasing magnetic field in agreement with the variations of the magnetization (Fig. 4) as shown in Table 2.

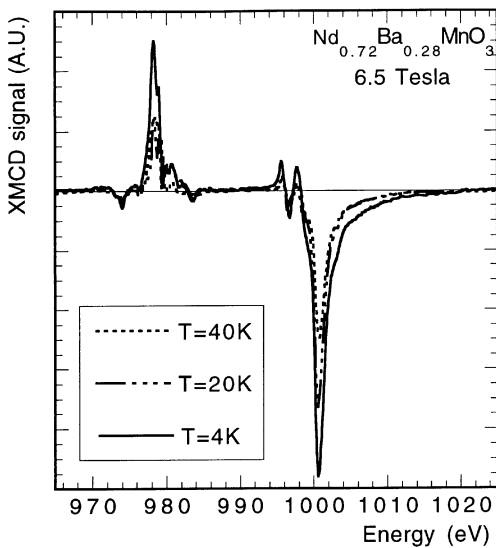


Fig. 10. Thermal variation of the XMCD signal of  $\text{Nd}_{0.72}\text{Ba}_{0.28}\text{MnO}_3$  at Nd  $M_{4/5}$ -edge.

Applying the sum rules to the dichroic signal, one can estimate the  $\langle L_z \rangle$  and  $\langle S_z \rangle$ . Components of the manganese magnetic moment  $\langle M_z \rangle$ . As shown above, only the first sum rule can be used and, since the two dichroic spectra were not taken simultaneously, one can only give a crude estimation of  $\langle L_z \rangle$ . Our calculation gives an estimation of  $\langle L_z \rangle$  (between  $-2.1 \times 10^{-2} \mu_B$  and  $-5.1 \times 10^{-2} \mu_B$ ) in agreement with the first calculation of Pellegrin [39].

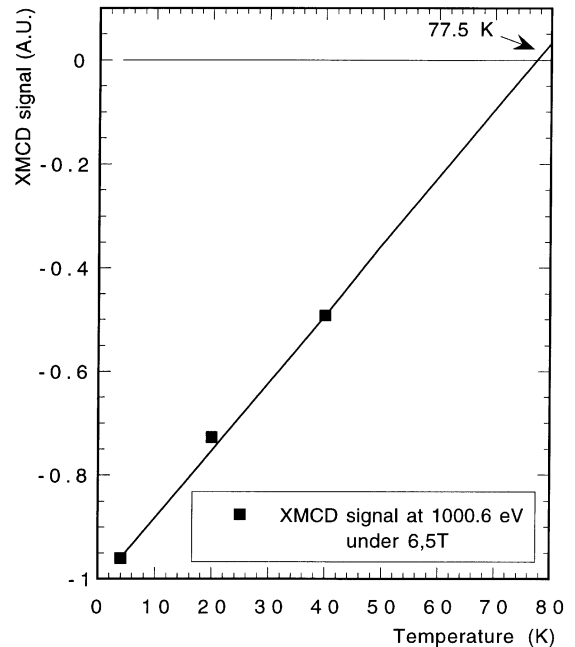


Fig. 11. Thermal variation of dichroic intensity at 1000.6 eV and 6.5 T with its linear extrapolation to zero giving an estimation of magnetic ordering temperature of neodymium subnetwork.

Table 2

Temperature (K)	Applied magnetic field (T)	XMCD signal at 642 eV	Magnetization value ( $\mu_B$ )
20	1.5	-0.20	1.07
20	3	-0.65	3.10
20	6.5	-0.72	4.16 <sup>a</sup>
130	1.5	-0.31	1.74
130	6.5	-0.54	2.79 <sup>a</sup>
300	< 5	No signal	< 0.80

<sup>a</sup>Recorded with an applied magnetic field equal at 5 T.

## 5. Conclusions

Dynamical Jahn–Teller distortions have been involved to explain the X-ray absorption spectroscopy data showing modification at  $T_c$ .

Moreover, XMCD data show a reversing on the orientation of the neodymium sublattice with respect to the manganese sublattice when the applied magnetic field is increased; magnetization measurements at high magnetic fields (5 T) could be interpreted as two ferromagnetically aligned sublattices.

The magnetic moments on neodymium may be related to the transition from a metallic state to a semi-conducting state which takes place below 80 K at 7 T and near 50 K at zero field. However, the magnetic moment on neodymium does not have any link with the magnetoresistance properties which are present at  $T = 140$  K whatever the applied magnetic field.

Now, it would be interesting to follow the magnetic moment on the neodymium cations by increasing the applied magnetic field for each photon energy scan at  $T = 20$  K to know the magnetic field at which the magnetic moment on the neodymium sublattice is reversed, and as a second part, it would be interesting to determine the Curie temperature of the neodymium sublattice.

## References

- [1] R.M. Kuster et al., *Physica B* 155 (1989) 362.  
 [2] R. Von Hemmolt et al., *Phys. Rev. Lett.* 71 (1993) 2331.  
 [3] H.L. Ju et al., *Appl. Phys. Lett.* 65 (1994) 2108.  
 [4] A. Maignan et al., *Solid State Commun.* 96 (1995) 623.  
 [5] R. Mahesh et al., *J. Solid State Chem.* 114 (1995) 297.  
 [6] S. Jin et al., *Appl. Phys. Lett.* 66 (1995) 382.  
 [7] B. Raveau et al., *J. Solid State Chem.* 130 (1997) 126.  
 [8] A. Maignan et al., *Mater. Res. Bull.* 32 (7) (1997) 965.  
 [9] A.P. Ramirez, *J. Phys.: Condens. Matter* 9 (1997) 8171.  
 [10] V. Caignaert et al., *Solid State Commun.* 95 (1995) 357.  
 [11] A. Maignan et al., *J. Mater. Chem.* 5 (7) (1995) 1089.  
 [12] B. Raveau et al., *J. Solid State Chem.* 117 (1995) 424.  
 [13] A. Maignan et al., *Z. Phys. B* 99 (1996) 305.  
 [14] H.Y. Hwang et al., *Phys. Rev. Lett.* 75 (5) (1995) 914.  
 [15] P.G. Radaelli et al., *Phys. Rev. B* 56 (13) (1997) 8265.  
 [16] F. Damay et al., *J. Appl. Phys.* 82 (1997) 6181.  
 [17] L.M. Rodriguez-Martinez et al., *Phys. Rev. B* 54 (22) (1996) R15622.  
 [18] F. Millange et al., *J. Solid State Chem.* 127 (1996) 131.  
 [19] V. Caignaert et al., *Phys. Rev. B*, accepted.  
 [20] M. Nevriiva et al., *Crystal Res. Technol.* 19 (2) (1984) 147.  
 [21] F. Fauth et al., *Physica B* 241 (1998) 427.  
 [22] G. Van Der Lann et al., *Phys. Rev. B* 34 (1986) 6529.  
 [23] G. Schutz et al., *Phys. Rev. Lett.* 58 (1987) 737.  
 [24] C. Giorgetti et al., *Phys. Rev. B* 48 (1993) 12732.  
 [25] G. Schutz, *Synchrotron Rad. News* 10 (4) (1997) 13.  
 [26] B.T. Thole et al., *Phys. Rev. Lett.* 68 (12) (1992) 1943.  
 [27] C.T. Chen et al., *Phys. Rev. Lett.* 75 (1) (1995) 152.  
 [28] M. Altarelli, Ph. Sainctavit, Sum rules of XMCD, in: *Magnetism and Synchrotron Radiation*, *Mittelwih*, 1996.  
 [29] E. Pellegrin, private communication.  
 [30] J.M. de Teresa et al., *Nature* 386 (1997) 256.  
 [31] F. Studer et al., *Proc. 9th Int. Conf. on X-Ray absorption fine structure*, *J. de Phys. IV* 7 (1997) C2–529.  
 [32] F. De Groot, thesis.  
 [33] V. Caignaert et al., *C.R. Acad. Sci.* 321 (1995) 515.  
 [34] D. Argyriou et al., *Phys. Rev. Lett.* 76 (1996) 3826.  
 [35] M. Hervieu et al., *Phys. Rev. B* 53 (14) (1996) 2774.  
 [36] V. Caignaert et al., *J. Magn. Magn. Mater.* 153 (1996) L260.  
 [37] J.L. Garcia-Munoz et al., *Phys. Rev. B* 55 (1) (1997) 34.  
 [38] A.J. Millis et al., *Phys. Rev. Lett.* 74 (1995) 5144.  
 [39] E. Pellegrin et al., *Proc. 9th Int. Conf. on X-ray absorption fine structure*, *J. Phys. IV* 7 (1997) C2–405.  
 [40] J. Goedkoop, thesis.  
 [41] G.J. Snyder et al., *Phys. Rev. B* 55 (10) (1997) 6453.  
 [42] Y. Moritomo et al., *Phys. Rev. B* 56 (19) (1997) 12190.  
 [43] A. Maignan et al., *Solid State Commun.* 107 (1998) 363.  
 [44] F. Millange et al., *Z. Phys. B* 101 (1996) 169.  
 [45] A. Sundaresan et al., *Phys. Rev. B* 56 (9) (1997) 5092.  
 [46] Ionic radii for twelve-fold coordination in oxides were taken from R.D. Shannon, *Acta Crystallogr. Sec. A* 32 (1976) 751.  
 [47] P. Carra et al., *Phys. Rev. Lett.* 70 (5) (1993) 694.  
 [48] Ph. Sainctavit, M.-A. Arrio, C.H. Brouder, *Phys. Rev. B* 52 (1995) 12766.  
 [49] A.J. Millis et al., *Phys. Rev. Lett.* 77 (1996) 175.